PHYSICAL REVIEW B **91**, 075413 (2015)

Two-photon interference from a quantum dot microcavity: Persistent pure dephasing and suppression of time jitter

Sebastian Unsleber,[1] Dara P. S. McCutcheon,[2] Michael Dambach,[1] Matthias Lermer,[1] Niels Gregersen,[2] Sven Höfling,[1,3] Jesper Mørk,[2] Christian Schneider,[1] and Martin Kamp[1]

[1]*Technische Physik and Wilhelm Conrad Röntgen Research Center for Complex Material Systems, Physikalisches Institut, Universität Würzburg, Am Hubland, D-97074 Würzburg, Germany*

[2]*Department of Photonics Engineering, Technical University of Denmark, Ørsteds Plads, 2800 Kgs. Lyngby, Denmark*

[3]*SUPA, School of Physics and Astronomy, University of St. Andrews, St. Andrews KY16 9SS, United Kingdom*

(Received 5 November 2014; revised manuscript received 21 January 2015; published 12 February 2015)

We demonstrate the emission of highly indistinguishable photons from a quasi-resonantly pumped coupled quantum dot–microcavity system operating in the regime of cavity quantum electrodynamics. Changing the sample temperature allows us to vary the quantum dot–cavity detuning and, on spectral resonance, we observe a threefold improvement in the Hong-Ou-Mandel interference visibility, reaching values in excess of 80%. Our measurements off-resonance allow us to investigate varying Purcell enhancements, and to probe the dephasing environment at different temperatures and energy scales. By comparison with our microscopic model, we are able to identify pure dephasing and not time jitter as the dominating source of imperfections in our system.

DOI: 10.1103/PhysRevB.91.075413 PACS number(s): 73.21.La

I. INTRODUCTION

Single indistinguishable photons are key to applications in quantum networks [1], linear optical quantum computing [2,3], and quantum teleportation [4,5]. One of the most promising platforms for single-photon sources is solid-state quantum dots (QDs) [6–10]. Compared to alternative platforms, such as cold atoms or trapped ions, single QDs offer several advantages: they can be driven electrically, which is of crucial importance for compact future applications [11–13], and, in principle, can be integrated in complex photonic environments and architectures, such as on-chip quantum optical networks [14,15]. When embedded in a bulk semiconductor, however, QDs suffer from poor photon extraction efficiencies, since only a minor fraction of the photons can leave the high refractive index material. This problem can be mitigated by integrating QDs into optical microcavities [12,16–18] or photonic waveguides [19–21], which can enhance extraction efficiencies to values beyond 50%.

In addition to increased extraction efficiencies, exploiting cavity quantum electrodynamics (cQED) effects in QD-based sources can have a positive effect on the interference properties (and hence the indistinguishability) of the emitted photon wave packets. Ideally, the wave packets emitted by an indistinguishable photon source are Fourier limited, with a recombination time T_1, and temporal extension of the wave packet given by $T_2 = 2T_1$ [22]. If additional dephasing channels with a characteristic time $1/\gamma$ exist, such as coupling to phonons or spectral diffusion, the coherence time is reduced according to $\frac{1}{T_2} = \frac{1}{2T_1} + \gamma$, which consequently leads to a reduction of the two-photon interference (TPI) visibility. It was theoretically shown that pure dephasing strongly affects the detuning dependence of the relative strength of the cavity and QD-emission peaks [23,24]. In the regime of cQED, the lifetime of the QD excitons can be manipulated via the photonic density of states in the cavity (the Purcell effect). If the timing of emission events is precisely known, and γ is constant, shortening of the emitter lifetime T_1 via the Purcell effect leads to an improved interference visibility as the condition $T_2 = 2T_1$ can be approximately restored [7,17,25]. This simple picture, however, is known to break down if there are uncertainties in the timing of emission events (time jitters) [26–28] or if the dephasing environment gives rise to more than a simple constant pure-dephasing rate, as is known to be the case for phonons [28–32]. As such, with the aim of designing improved single indistinguishable photon sources, it is crucially important to first establish the magnitude of time jitters and the nature of any dephasing environments.

In this work, we exploit a microcavity with a high Purcell factor and weak nonresonant contributions of spectator QDs to probe the interference properties of photons emitted from a single QD as a function of the QD-cavity detuning. In contrast to previous studies, where nonresonant coupling to spectator QDs [33] or strong temperature-induced dephasing [25] dominated the experiments, we observe a strong improvement of the two-photon visibility on resonance, which exceeds a factor of three compared to the off-resonant case. We extend the theoretical model of Ref. [28] to derive an expression for the Hong-Ou-Mandel dip, including the effects of both time jitter and pure dephasing on- and off-resonance. This allows us to reject timing jitter and definitively attribute sources of pure dephasing as the dominant factor limiting the indistinguishability of our photons. Furthermore, we show that the degree of symmetry we observe for positive and negative detuning suggests pure dephasing caused by both phonon coupling and spectral diffusion.

II. QUANTUM DOT–CAVITY SYSTEM

The device under investigation comprises a QD embedded in a micropillar cavity with a quality factor of $Q = 3200$. The layer structure consists of 25 (30) alternating $\frac{\lambda_C}{4 \cdot n}$-thick GaAs/AlAs mirror pairs which form the upper (lower) distributed Bragg reflector (DBR). The cavity region is composed of six alternating GaAs/AlAs layers with decreasing (lower part) and increasing (upper part) thickness. A single layer of partially capped and annealed InAs QDs is integrated

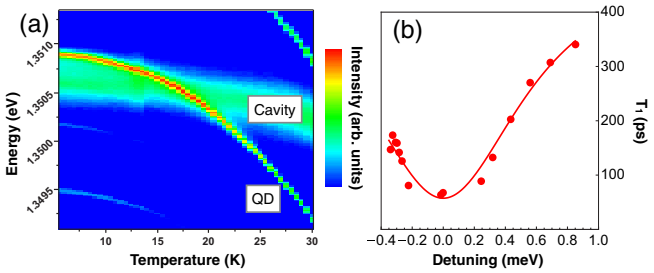

FIG. 1. (Color online) (a) Temperature-dependent intensity map of the QD-cavity system. The QD reaches spectral resonance with the cavity mode at $T = 17.5$ K. (b) QD lifetime as a function of QD-cavity detuning. The fit is a Lorentzian profile where the linewidth is fixed to the cavity linewidth. A Purcell enhancement of $F_P = 7.8 \pm 2.3$ is extracted.

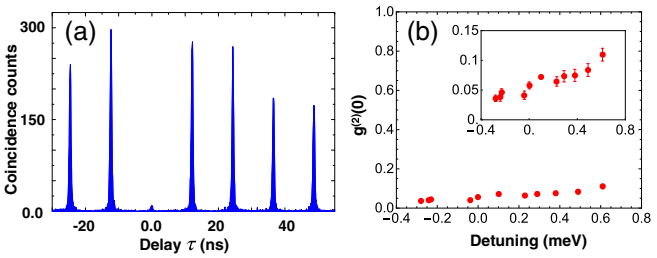

FIG. 2. (Color online) (a) Autocorrelation histogram on QD-cavity resonance, from which we extract $g^{(2)}(0) = (0.058 \pm 0.006)$. (b) Autocorrelation function as a function of QD-cavity detuning (the inset shows a zoom-in of the y axis).

in the central layer of the tapered segment, i.e., in the vertical maximum of the optical field [34]. Micropillars with varying diameters were etched into the wafer (the pillar under investigation has a diameter of 1050 nm) to provide zero dimensional mode confinement. As a result of the Bloch mode engineering [34], our micropillars support optical resonances with comparably large quality factors down to the submicron diameter range, which yields the possibility to significantly increase the Purcell factor in such microcavities compared to conventional DBR resonators based on λ-thick cavity spacers. The sample was placed inside an optical cryostat, and the QD was excited via a picosecond-pulsed Ti:sapphire laser with a repetition frequency of 82 MHz (pulse separation 12.2 ns). The laser beam was coupled into the optical path via a polarizing beam splitter, which also suppresses the scattered laser light from the detection path of the setup. Further filtering was implemented by a long-pass filter in front of the monochromator. After spectral filtering, the emitted photons were coupled into a polarization maintaining single-mode fiber followed by a fiber-coupled Mach-Zehnder interferometer (MZI) with a variable fiber-coupled time delay in one arm to measure the TPI in a Hong-Ou-Mandel (HOM) setup. The second beam splitter of the MZI can be removed to directly measure the autocorrelation function of the signal.

Figure 1(a) shows the temperature-dependent micropho-toluminescence (μ-PL) map of the investigated QD-cavity system, which was recorded under nonresonant excitation conditions. The QD-emission line, which we attribute to the neutral exciton, can be tuned through the cavity mode by changing the sample temperature. Spectral resonance with the fundamental cavity mode is achieved at $T = 17.5$ K. Due to the Purcell enhancement, the integrated intensity of the QD increases by a factor of more than three when the QD and cavity are tuned into resonance. In order to directly and accurately extract the Purcell factor of our coupled system, we measured the exciton lifetime via time-resolved μ-PL as a function of the QD-cavity detuning (see Appendix A 2). As seen in Fig. 1(b), we observe a strong decrease of the lifetime when the QD is tuned into resonance as a result of the Purcell effect. The Purcell factor $F_P = \frac{T_1(\Delta\to\infty)}{T_1(\Delta\to 0)} - 1$ [35] is extracted by fitting the data with a Lorentzian profile (the width being fixed to the cavity linewidth $\kappa = 0.42$ meV), and we find a value as high as $F_P = 7.8 \pm 2.3$ as a result of the small mode volume of our microcavity.

We now study the single-photon emission properties of our system, which is particularly important on-resonance, where the single-photon characteristics can be deteriorated by nonresonant contributions to the cavity from spectator QDs, or luminescence from the background continuum funneled into the cavity mode [36]. The second-order photon autocorrelation was probed under quasiresonant excitation conditions, with a laser tuned 32 meV to the high-energy side of the single-exciton emission feature, with a (below-saturation) power of 311 μW. The on-resonance ($T = 17.5$ K) autocorrelation histogram is shown in Fig. 2(a). The strongly suppressed peak around $\tau = 0$ is a clear signature of single-photon emission. We extract the $g^{(2)}(\tau = 0)$ value by dividing the area of the central peak by the average area of all the side peaks, leading to $g^{(2)}(0) = 0.058 \pm 0.006$, reflecting the high purity of our cavity-enhanced single-photon source. Off-resonance we find a minimum value of $g^{(2)}(0) = (0.036 \pm 0.005)$ at $\Delta = -0.28$ meV ($T = 6.4$ K). For increasing temperatures, we note a modest increase up to $g^{(2)}(0) = (0.11 \pm 0.01)$ for $\Delta = 0.61$ meV ($T = 25.5$ K). This value is still close to perfect single-photon emission, and we attribute the slight rise to a lowered signal to background ratio between QD and cavity emission. We note that no deterioration of the $g^{(2)}(0)$ value can be observed on spectral resonance, which suggests only very weak contributions from spectator QDs to the cavity signal.

III. PHOTON INDISTINGUISHABILITY

We now assess the indistinguishable nature of the emitted photons, which we probe in the HOM interferometer under the same pulsed quasiresonant excitation conditions. The second-order correlation histogram for zero time delay in the MZI for the resonant case is shown in Fig. 3(a). Strong suppression of the central correlation peak directly reflects a strong degree of photon indistinguishability. The black markers in Fig. 3(b) are obtained by dividing the area of the peak centered around $\tau = 0$ by that centered around $\tau = 24$ ns for various time delays τ_D, and we observe a clear HOM dip. For large time delays τ_D, the correlation values slightly exceed 0.5 as a result of the finite two-photon emission probability, as seen in Fig. 2. We correct the interference data by subtracting half the corresponding experimentally extracted on-resonance value of $g^{(2)}(0) = (0.058 \pm 0.006)$

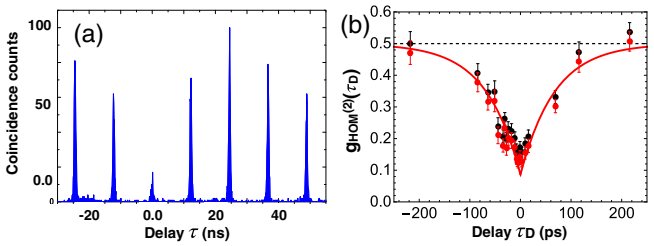

FIG. 3. (Color online) (a) Histogram of the TPI for zero time delay between the two arms of the interferometer, from which we extract $g^{(2)}_{\mathrm{HOM}}(0) = 0.17 \pm 0.02$. (b) Measured two-photon interference vs the time delay. The measurement shows the clear HOM dip (black dots). Due to a nonvanishing two-photon probability, the data points go slightly above 0.5 for large τ_D. These are corrected by subtracting half the measured $g^{(2)}(0)$ value on resonance shown in Fig. 2 (red markers). These corrected data were fitted to extract a visibility of $\nu = (83 \pm 5)\%$.

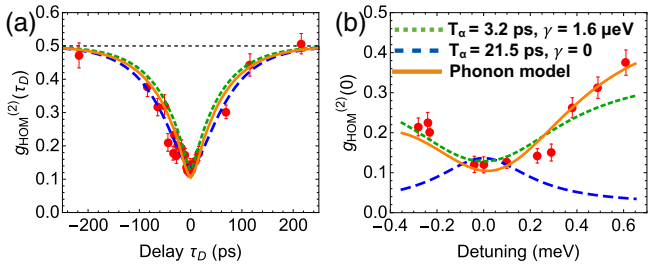

FIG. 4. (Color online) (a) HOM dip and HOM-dip depth as a function of detuning (b). The dashed blue curves correspond to a parameter set for which time jitter dominates, which we find to be inconsistent with the data off-resonance shown in (b). The dotted green curves correspond to a parameter set for which pure dephasing dominates, which is able to consistently reproduce all data. The solid orange curves again correspond to a parameter set dominated by pure dephasing, but where 40% of the dephasing on-resonance is caused by coupling to phonons.

(red markers) (see Appendix B 2). We then fit our data to the function $g^{(2)}_{\mathrm{HOM}}(\tau_D) = 0.5(1 - \nu \exp[-|\tau_D|/T_1])$, where we set $T_1 = 67$ ps [see Fig. 1(b)], and we find a visibility of $\nu = 83 \pm 5\%$. This high value is a direct consequence of the large Purcell factor in our high-quality QD-cavity system.

To further analyze our experimental data and, in particular, to determine the relative influences of time jitter and pure dephasing on the indistinguishability of the emitted photons, we extend the theory of Ref. [28] to derive an expression for the TPI as a function of both time delay τ_D and detuning. Dephasing caused by coupling to phonons is known to affect the TPI properties of the emission from a QD-cavity system in a highly nontrivial way, giving rise, for example, to pronounced asymmetries for positive and negative QD-cavity detunings [28–30]. We find, however, that nearly all features seen in our data can be well reproduced by a model assuming a simple constant pure-dephasing rate. We present this simplified model first, and then go on to show that by including phonons in a rigorous manner at a Hamiltonian level, the behavior off-resonance allows us to approximately determine the relative influence of phonons as compared to other sources of dephasing.

We model the QD as a three-level system, and consider the vacuum and single-photon Fock states of the cavity. Provided the QD-cavity coupling strength is sufficiently weak and/or the cavity decay rate is sufficiently large, the cavity degrees of freedom can be adiabatically eliminated from the equations of motion for the QD-cavity system [28]. The result is a master equation of the form (see Appendix B 3)

$$\frac{d\rho}{dt} = -\frac{i}{\hbar}[\Delta\,|E\rangle\langle E|\,,\rho] + (L_\Gamma(|G\rangle\langle E|) + L_{2\gamma}(|E\rangle\langle E|) + L_\alpha(|E\rangle\langle P|))\rho, \quad (1)$$

where the states $|E\rangle = |e,n=0\rangle$, $|G\rangle = |g,n=1\rangle$, $|P\rangle = |p,n=0\rangle$ represent the QD in ground (g), single-exciton state (e), or pump level (p), with the cavity containing zero or one excitation. The QD-cavity detuning is Δ, while γ is the pure-dephasing rate, and α is the rate at which the pump level decays into the single-exciton state, with $T_\alpha = 1/\alpha$ determining the magnitude of the time jitter (i.e., $T_\alpha = 0$ represents the ideal case in which there is no time jitter). The Purcell enhanced spontaneous-emission rate is

$$\Gamma = T_1^{-1} = \Gamma_B + 2g^2\frac{\gamma_{\mathrm{tot}}}{\gamma_{\mathrm{tot}}^2 + \Delta^2}, \quad (2)$$

with Γ_B the background decay rate, g the QD-cavity coupling strength, and $\gamma_{\mathrm{tot}} = \gamma + \frac{1}{2}(\kappa + \Gamma_B)$ with κ the cavity decay rate. The validity of Eq. (1) relies on the condition $\gamma_{\mathrm{tot}} \gg \Delta, \Gamma, g$, which is satisfied in all our experiments.

Equation (1) can then be used to derive an expression for the normalized coincidence events in the TPI measurements (for details, see Appendix B 3). The second-order correlation function for the HOM interference measurements is found to read

$$g^{(2)}_{\mathrm{HOM}}(\tau_D) = \frac{1}{2}\left(1 - \frac{\nu}{\Gamma - \alpha}[\Gamma e^{-|\tau_D|\alpha} - \alpha e^{-|\tau_D|\Gamma}]\right), \quad (3)$$

where the detuning dependence enters through Γ [see Eq. (2)], and $\nu = [\Gamma/(\Gamma + 2\gamma)][\alpha/(\Gamma + \alpha)]$ is the visibility. We note that while the expression for ν has been derived before [28], Eq. (3) is able to describe the full behavior of the HOM dip for nonzero values of τ_D including time jitter and pure dephasing. This model provides us with simple analytical expressions with which we can fit the experimental TPI data. Crucially, it allows us to explore how a given set of parameters simultaneously affects the HOM dip *and* the TPI visibility as the QD and cavity are moved off-resonance.

In Fig. 4(a), we show again the HOM dip, while in Fig. 4(b), we show the depth of the HOM dip as a function of detuning. We see a pronounced rise of the HOM dip as the QD is brought out of resonance, corresponding to visibilities on- and off-resonance which differ by more than a factor of three. The dashed blue curves in Fig. 4 show a fit to Eq. (3) where only the data in Fig. 4(a) (the HOM dip) are considered. Fitting parameters $T_\alpha = 1/\alpha = 21.5$ ps and $\gamma = 0$ μeV are found, corresponding to a regime where time jitter dominates. These parameters are able to reproduce the HOM dip well, but fail to describe the data off-resonance. Indeed, we find that if we simultaneously fit all the data shown in Fig. 4, we find parameters $T_\alpha = 1/\alpha = 3.2$ ps and

$\gamma = 1.6$ μeV, corresponding to a regime for which pure dephasing dominates. These parameters are shown by the dotted green curves, and much better agreement is found. These two fits show that while both time jitter and pure dephasing affect the shape of the HOM dip in a similar way, the reduction in the visibility seen off-resonance can only be explained by a system in which pure dephasing dominates. As the QD and cavity are moved off-resonance, the Purcell effect weakens (see Fig. 1) and $\Gamma = 1/T_1$ decreases. For a source dominated by pure dephasing, the visibility is given by $\nu \approx \Gamma/(\Gamma + 2\gamma)$, and a reduction in Γ causes a reduction in ν. For a source dominated by time jitter, the visibility instead follows $\nu \approx \alpha/(\Gamma + \alpha)$, and a reduction in Γ increases ν. We stress that which of the two regimes is relevant for a particular system has important consequences for how experimental modifications will translate to improvements in photon indistinguishabilities. In the present case, since pure dephasing dominates, a complete elimination of time jitters (achieved, for example, via strictly resonant excitation conditions) will lead to only a modest 4% increase in the visibility, while an elimination of sources of pure dephasing will lead to an increase of 20% up to $\nu = 95\%$.

IV. DISCUSSION

The low value of $T_\alpha = 3.2$ ps implies that our quasiresonant excitation scheme leads to a very fast relaxation to the desired single-exciton state. This is also supported by the laser detuning we use (32 meV), which corresponds to the energy of a longitudinal optical phonon, known to relax on this time scale [37]. We attribute pure dephasing in our sample as caused by exciton-phonon coupling and spectral fluctuation of the QD energy levels on a time scale shorter than the pulse separation of 12.2 ns. The constant pure-dephasing rate used in our theory is expected to well approximate the spectral fluctuations, but the influence of phonons is known to give rise to more complicated behavior [28–31]. In particular, differing phonon absorption and emission rates at low temperatures are expected to lead to asymmetries for positive and negative detuning [29]. By including phonons using a time-convolutionless master-equation technique (see, e.g., Ref. [28] or Appendix B 5), we find that these asymmetries can improve our fits. The solid orange curves in Fig. 4 show the predictions of a parameter set similar to that of the dotted green curve, but where we have included phonons with a strength corresponding to approximately 40% of the total pure-dephasing on-resonance [38], and it can be seen that the phonon contribution improves the fits to the data. We note, however, that when increasing the phonon contribution even further, the fits become worse as the asymmetry becomes too strong. The relatively strong symmetry seen in Fig. 4(b) therefore leads us to conclude that both phonons and additional sources of constant pure dephasing (such as a spectral diffusion) are present in our system.

In conclusion, we have demonstrated the feasibility of our cavity design to enhance the emission of indistinguishable single photons generated in epitactically grown InAs QDs. Using a quasiresonant excitation scheme, we were able to show a TPI visibility as high as $\nu = (83 \pm 5)\%$ and a two-photon emission probability as low as $g^{(2)}(0) = (0.036 \pm 0.005)$. We studied the influence of the QD-cavity detuning on both the two-photon probability and the degree of indistinguishability of the emitted photons. The TPI measurements are explained by our theory, which takes the QD-cavity detuning, time jitter, and pure dephasing into account, and which identifies sources of pure dephasing as the ultimate factor limiting the indistinguishably of emitted photons.

ACKNOWLEDGMENTS

The authors would like to thank M. Emmerling and A. Wolf for sample preparation. We acknowledge financial support by the State of Bavaria and the German Ministry of Education and Research (BMBF) within the projects Q.com-H, the Chist-era project SSQN, as well as the Villum Fonden via the NATEC Centre of Excellence. This work was additionally funded by project SIQUTE (Contract No. EXL02) of the European Metrology Research Programme (EMRP). The EMRP is jointly funded by the EMRP participating countries within EURAMET and the European Union. S.H. gratefully acknowledges support by the Royal Society and the Wolfson Foundation.

APPENDIX A: EXPERIMENTAL METHODS

1. Coherence measurements

In addition to the Hong-Ou-Mandel (HOM) interference measurements, the coherence of the emitted photons was measured using a free-beam unbalanced Michelson interferometer. One mirror is mounted on a 300-mm-long linear stage, which defines the path-length difference between both optical arms, and, by using an additional implemented piezo crystal at one mirror, the interference fringe contrast from the emitted photons is measured as a function of the path-length difference. The measurements (black data points) are shown in Fig. 5(a) for a QD in spectral resonance with the cavity mode. Fitting these data points to a Gaussian function of the form $A + B * \exp[-(\pi/2)(\tau/T_2)^2]$, we extract a coherence time of $T_2 = (93 \pm 3)$ ps. This value in slightly lower than the coherence time extracted from the HOM dip in Fig. 3, for which

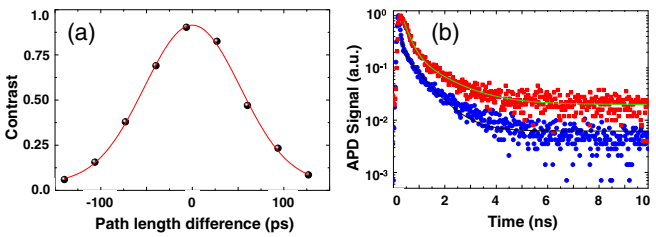

FIG. 5. (Color online) (a) Coherence length measurement using a free-beam unbalanced Michelson interferometer. Fitting the data points with a Gaussian distribution (red solid curve), we extract a coherence time of $T_2 = (93 \pm 3)$ ps. (b) Time-resolved μ-PL measurements. The blue dotted data points correspond to spectral resonance between the QD and fundamental cavity mode ($\Delta = 0$ meV), while the red square points were taken for a detuning of $\Delta = 0.61$ meV. The solid curves correspond to fits to a biexponential function, from which we extract $T_1 = (67 \pm 8)$ ps on-resonance and $T_1 = (306 \pm 13)$ ps off-resonance.

$T_2 = 111$ ps. We attribute this slight discrepancy to a long-term spectral jitter which affects the QD emission energy on time scales which are longer than the pulse separation. In the HOM measurement, only subsequently emitted photons separated by 12.2 ns (the laser pulse separation) contribute to the measured indistinguishability, and hence the inferred coherence time of $T_2 = 111$ ps. The HOM measurements therefore include an effective time filter. In contrast, the measurements made using the Michelson interferometer are time integrated and, as such, long-term drifts and spectral diffusion result in a deterioration of the extracted T_2 value [7,9,39].

2. Lifetime measurements

In order to measure the lifetime of the QD emission, we couple the spectrally filtered photons into a single-mode fiber attached to an avalanche photodiode (APD) with resolution ~40 ps. Figure 5(b) shows two representative time-resolved measurements of the QD emission under quasiresonant excitation. The blue round data points correspond to spectral resonance between the QD and fundamental cavity mode ($\Delta = 0$ meV), while the red square data points correspond to a detuning of $\Delta = 0.61$ meV. The measurements (time window 100 ns) each contain six complete decay curves similar to those shown in Fig. 5(b), which we fit to a biexponential decay function. The shorter time constant represents the lifetime of the bright exciton, while the longer time originates from a dark exciton effect. For the decay curves in Fig. 5(b), we find $T_1 = (67 \pm 8)$ ps on-resonance and $T_1 = (306 \pm 13)$ ps for $\Delta = 0.61$ meV.

APPENDIX B: TWO-PHOTON INTERFERENCE THEORY

Here we provide the necessary background for the theoretical analysis of the data presented in the main text.

1. Hanbury Brown and Twiss measurements

We first consider the Hanbury Brown and Twiss (HBT) experimental setup used to measure the two-photon emission probability of our source. Emission from the source is incident upon a 50:50 beam splitter, and two detectors are placed equidistantly on the two output arms. We label t_1 the time of the detection event at detector 1, and t_2 that of detector 2. The probability of detecting a photon at detector 1 at t_1, and at detector 2 at t_2, is proportional to the second-order field correlation function,

$$G^{(2)}(t_1,t_2) = \langle b_1^\dagger(t_1) b_2^\dagger(t_2) b_2(t_2) b_1(t_1)\rangle, \tag{B1}$$

where $b_1^\dagger(t)$ is the creation operator for the mode propagating to detector 1 in the Heisenberg picture, and similarly for $b_2^\dagger(t)$. We relate these modes to those on the input arms, described by creation operators $a_1^\dagger$ and $a_2^\dagger$, using the unitary mode transformation [26],

$$\begin{pmatrix} b_1^\dagger(t) \\ b_2^\dagger(t) \end{pmatrix} = \frac{1}{\sqrt{2}} \begin{pmatrix} 1 & 1 \\ -1 & 1 \end{pmatrix} \begin{pmatrix} a_1^\dagger(t-\tau_D) \\ a_2^\dagger(t) \end{pmatrix}, \tag{B2}$$

where τ_D is the delay introduced between arrival times at the beam splitter. For the HBT measurement, there is no input in arm 1, and we simply have $G^{(2)}(t_1,t_2) \to G^{(2)}_{\mathrm{HBT}}(t_1,t_2)$, with

$$G^{(2)}_{\mathrm{HBT}}(t_1,t_2) = \tfrac{1}{4}\langle a^\dagger(t_1) a^\dagger(t_2) a(t_2) a(t_1)\rangle, \tag{B3}$$

where the subscripts on the operators have been dropped since they are all equal.

To measure the two-photon emission probability $g^{(2)}(0)$, we integrate Eq. (B3) over all t_1 and t_2, and divide this area by an adjacent peak. The adjacent peaks correspond to Eq. (B3), but where t_1 and t_2 differ sufficiently that mode operators at these times are completely uncorrelated. This gives the uncorrelated coincidence probability in the HBT measurement $G^{(2)}_{\mathrm{HBT,UC}}(t_1,t_2) = (1/4)\mathcal{G}^{(2)}(t_1,t_2)$, with

$$\mathcal{G}^{(2)}(t_1,t_2) = \langle a^\dagger(t_1) a(t_1)\rangle \langle a^\dagger(t_2) a(t_2)\rangle. \tag{B4}$$

The normalized autocorrelation function is then defined as

$$\begin{aligned} g^{(2)}(0) &= \frac{\int_{-\infty}^{\infty} dt_1 \int_{-\infty}^{\infty} dt_2 G^{(2)}_{\mathrm{HBT}}(t_1,t_2)}{\int_{-\infty}^{\infty} dt_1 \int_{-\infty}^{\infty} dt_2 G^{(2)}_{\mathrm{HBT,UN}}(t_1,t_2)} \\ &= \frac{\int_{-\infty}^{\infty} dt_1 \int_{-\infty}^{\infty} dt_2 \langle a^\dagger(t_1) a^\dagger(t_2) a(t_2) a(t_1)\rangle}{\int_{-\infty}^{\infty} dt_1 \int_{-\infty}^{\infty} dt_2 \langle a^\dagger(t_1) a(t_1)\rangle \langle a^\dagger(t_2) a(t_2)\rangle}, \end{aligned} \tag{B5}$$

which is equal to zero for $\langle a^\dagger(t_1) a^\dagger(t_2) a(t_2) a(t_1)\rangle = 0$.

2. Hong-Ou-Mandel experiment

We now consider the Hong-Ou-Mandel (HOM) experimental setup used to measure the indistinguishable nature of the emitted photons. Two emission events are incident on a 50:50 beam splitter, with a delay τ_D introduced into input arm one. The unnormalized probability of a coincidence event is again given by Eq. (B1), and the beam splitter is described by Eq. (B2). Upon combining these equations, we find 16 terms. These can be simplified by assuming that modes 1 and 2 are identical but statistically independent, which allows us to write $\langle A_1 A_2\rangle = \langle A_1\rangle\langle A_2\rangle$, where A_1 is any product of mode operators pertaining to mode 1, and similarly for A_2. We then find eight terms linear in $\langle a_1\rangle$ and $\langle a_2\rangle$. For an electromagnetic field state of the form $\sum_n a_n |n\rangle\langle n|$, with $|n\rangle$ a Fock state, expectation values linear in the ladder operators are zero, and we neglect these terms. This leaves second- and fourth-order terms. The second-order terms involve expectation values of the form $\langle a^\dagger(t_1) a^\dagger(t_2)\rangle$, which also give zero for electromagnetic fields, as discussed above. The remaining terms give

$$\begin{aligned} G^{(2)}_{\mathrm{HOM}}(t_1,t_2,\tau_D) = {} & G^{(2)}_{\mathrm{HBT}}(t_1-\tau_D,t_2-\tau_D) + G^{(2)}_{\mathrm{HBT}}(t_1,t_2) \\ & + \tfrac{1}{4}\{\mathcal{G}^{(2)}(t_1-\tau_D,t_2) + \mathcal{G}^{(2)}(t_1,t_2-\tau_D) \\ & - 2\mathrm{Re}[G^{(1)}(t_1-\tau_D,t_2-\tau_D) G^{(1)}(t_2,t_1)]\}, \end{aligned} \tag{B6}$$

where $G^{(1)}(t_1,t_2) = \langle a^\dagger(t_1) a(t_2)\rangle$ is the unnormalized first-order correlation function.

To normalize this quantity, we again consider the scenario in which t_1 and t_2 are sufficiently separated that mode operators evaluated at these two times are uncorrelated. In doing so, we find the uncorrelated coincidence probability for the HOM setup, $G^{(2)}_{\mathrm{HOM,UC}}(t_1,t_2) = \frac{1}{4}[\mathcal{G}^{(2)}(t_1,t_2) + \mathcal{G}^{(2)}(t_1-\tau_D,t_2) + \mathcal{G}^{(2)}(t_1,t_2-\tau_D) + \mathcal{G}^{(2)}(t_1-\tau_D,t_2-\tau_D)]$. Since we

integrate over all t_1 and t_2, the appearances of τ_D can be neglected, i.e., we have

$$\int_{-\infty}^{\infty} dt_1 \int_{-\infty}^{\infty} dt_2 G^{(2)}_{\mathrm{HOM,UC}}(t_1,t_2) = \int_{-\infty}^{\infty} dt_1 \int_{-\infty}^{\infty} dt_2 \mathcal{G}^{(2)}(t_1,t_2) \tag{B7}$$

by a simple change of variables. An identical argument can be made for the τ_D appearing in $G^{(2)}_{\mathrm{HBT}}(t_1-\tau_D,t_2-\tau_D)$ in Eq. (B6). In the HOM setup, we therefore measure the normalized quantity,

$$\begin{aligned} g^{(2)}_{\mathrm{HOM}}(\tau_D) &= \frac{\int_{-\infty}^{\infty} dt_1 \int_{-\infty}^{\infty} dt_2 G^{(2)}_{\mathrm{HOM}}(t_1,t_2,\tau_D)}{\int_{-\infty}^{\infty} dt_1 \int_{-\infty}^{\infty} dt_2 G^{(2)}_{\mathrm{HOM,UN}}(t_1,t_2)} \\ &= \frac{1}{2} g^{(2)}_{\mathrm{HBT}}(0) + \frac{1}{2}[1 - C(\tau_D)], \end{aligned} \tag{B8}$$

where we have defined the strictly two-photon coalescence probability,

$$C(\tau_D) = \frac{\int_{-\infty}^{\infty} dt_1 \int_{-\infty}^{\infty} dt_2 \mathrm{Re}[G^{(1)}(t_1-\tau_D,t_2-\tau_D) G^{(1)}(t_2,t_1)]}{\int_{-\infty}^{\infty} dt_1 \int_{-\infty}^{\infty} dt_2 \mathcal{G}^{(2)}(t_1,t_2)}, \tag{B9}$$

which for $\tau_D = 0$ becomes the visibility $v = C(0)$.

3. Quantum dot–cavity system

We now develop a master equation which will allow us to derive an analytic expression for $g^{(2)}_{\mathrm{HOM}}(\tau_D)$ in the presence of time jitter and pure dephasing. We follow Ref. [28] and model the quantum dot (QD) as a three-level system, with crystal ground state $|g\rangle$, single-exciton state $|e\rangle$, and pump level $|p\rangle$, having energies $\hbar\omega_g$, $\hbar\omega_e$, and $\hbar\omega_p$, respectively. The cavity mode is described by creation and annihilation operators $c^\dagger$ and c, and has frequency ω_c. The system is depicted in Fig. 6. In a rotating frame, the QD-cavity system is described by the Jaynes-Cummings Hamiltonian,

$$H_{\mathrm{JC}} = \hbar\Delta\, |e\rangle\langle e| + \hbar g(|e\rangle\langle g|\, c + |g\rangle\langle e|\, c^\dagger), \tag{B10}$$

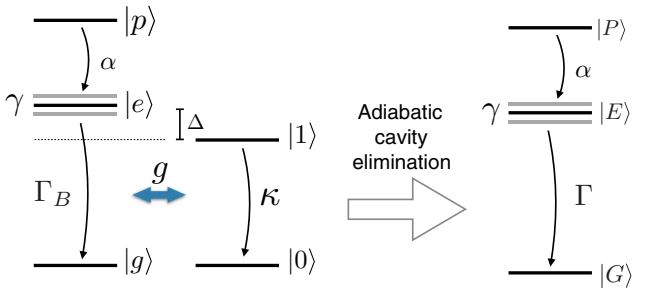

FIG. 6. (Color online) Schematic diagram of the system under consideration; a quantum dot with pump level $|p\rangle$, excited state $|e\rangle$, and ground state $|g\rangle$ couples to a cavity mode with strength g and detuning Δ. We consider only the zero-photon and one-photon manifolds of the cavity mode, which decays with rate κ. The $|p\rangle \to |e\rangle$ transition has rate α, while the spontaneous-emission process of $|e\rangle \to |g\rangle$ has background rate Γ_B. The excited state undergoes pure dephasing with rate γ. Adiabatic cavity elimination results in an effective three-level system with a modified spontaneous-emission rate Γ.

where $\Delta = (\omega_e - \omega_g) - \omega_c$ is the detuning of the QD transition from the cavity mode, and g is the QD-cavity coupling strength. Relaxation processes are added using the Lindblad formalism [40], and the master equation describing the QD-cavity degrees of freedom ρ becomes

$$\begin{aligned} \frac{d\rho}{dt} = &-\frac{i}{\hbar}[H_{\mathrm{JC}},\rho] + [L_\kappa(c) + L_{\Gamma_B}(|g\rangle\langle e|) \\ &+ L_{2\gamma}(|e\rangle\langle e|) + L_\alpha(|e\rangle\langle p|)]\rho, \end{aligned} \tag{B11}$$

where the Lindblad operators satisfy $L_\gamma(A)\rho = \gamma(A\rho A^\dagger - \frac{1}{2}\{A^\dagger A,\rho\})$, with α and κ the decay rates of the pump level and cavity, respectively. The background spontaneous-emission rate of the QD is Γ_B, and the rate γ describes pure dephasing of the QD excited-state level.

In the limit of weak QD-cavity coupling and/or strong cavity decay, the cavity can be adiabatically eliminated from equations of motion describing our system. Formally, we require $\gamma_{\mathrm{tot}} \gg \Delta, \Gamma, g$ with $\gamma_{\mathrm{tot}} = \gamma + \frac{1}{2}(\kappa + \Gamma)$, and provided we consider the initial state $\rho(0) = |p\rangle\langle p|\, |0\rangle\langle 0|$, with $|0\rangle$ the vacuum state of the cavity mode, the dynamics can be well approximated by the master equation [28]

$$\begin{aligned} \frac{d\rho}{dt} = &-\frac{i}{\hbar}[\Delta\, |E\rangle\langle E|\,,\rho] + [L_\Gamma(|G\rangle\langle E|) \\ &+ L_{2\gamma}(|E\rangle\langle E|) + L_\alpha(|E\rangle\langle P|)]\rho, \end{aligned} \tag{B12}$$

which is Eq. (1) in the main text.

4. Photon indistinguishability for the QD-cavity system

We now use Eq. (B12) to calculate the TPI probability, given by Eq. (B8). To proceed, we note that in the far field, we can make the replacement $a(t) \to \sigma(t)$ with $\sigma = |G\rangle\langle E|$ [26] in Eq. (B8). Then, to calculate the second-order correlation function $G^{(2)}_{\mathrm{HBT}}(t_1,t_2) = \frac{1}{4}\langle a^\dagger(t_1)a^\dagger(t_2)a(t_1)a(t_2)\rangle \to \frac{1}{4}\langle \sigma^\dagger(t_1)\sigma^\dagger(t_2)\sigma(t_1)\sigma(t_2)\rangle$, we make use of the quantum regression theorem to write [41]

$$\frac{\partial}{\partial\tau} G^{(2)}_{\mathrm{HBT}}(t,t+\tau) = -\Gamma\, G^{(2)}_{\mathrm{HBT}}(t,t+\tau). \tag{B13}$$

For $\tau = 0$, we find $G^{(2)}_{\mathrm{HBT}}(t,t) = 0$ since $\sigma^2 = (\sigma^\dagger)^2 = 0$, and, as such, $G^{(2)}_{\mathrm{HBT}}(t,t+\tau) = 0$ and we can set $g^{(2)}(0) = 0$ in Eq. (B8). This reflects that for the theory presented here, we have strictly one (or less) excitations in the system at any time.

We now calculate the two-photon coalescence probability expressed in Eq. (B9). To begin, we consider the uncorrelated probability $\mathcal{G}^{(2)}(t_1,t_2) \to \langle\sigma^\dagger(t_1)\sigma(t_1)\rangle\langle\sigma^\dagger(t_2)\sigma(t_2)\rangle$. The quantity $\langle\sigma^\dagger(t)\sigma(t)\rangle = \mathrm{Tr}[\rho(t)\sigma^\dagger\sigma]$ is just the excited-state population at time t, and from Eq. (B12), we have

$$\langle\sigma^\dagger(t)\sigma(t)\rangle = \Theta(t)\frac{\alpha}{\Gamma-\alpha}(e^{-\alpha t} - e^{-\Gamma t}), \tag{B14}$$

where the Heaviside θ function [$\Theta(t) = 0$ for $t < 0$ and $\Theta(t) = 1$ for $t > 0$] has been introduced to ensure no excitations are present before emission events. From the quantum regression theorem, the first-order correlation function $G^{(1)}(t,t+\tau)$ obeys the equation of motion,

$$\frac{\partial}{\partial\tau} G^{(1)}(t,t+\tau) = -\left(\gamma + \frac{1}{2}\Gamma + i\Delta\right) G^{(1)}(t,t+\tau), \tag{B15}$$

with initial condition $G^{(1)}(t,t) = \langle\sigma^\dagger(t)\sigma(t)\rangle$, which gives

$$G^{(1)}(t,t+\tau) = \langle\sigma^\dagger(t)\sigma(t)\rangle e^{-(\gamma+\frac{1}{2}\Gamma+i\Delta)|\tau|}. \quad \text{(B16)}$$

Finally, performing the integrals in Eq. (B8), we arrive at Eq. (3) in the main text.

5. Exciton-phonon coupling

To explore the influence of phonons seen in our data, a weak exciton-phonon coupling time-convolutionless master-equation technique is used [28]. To second order in the exciton-phonon coupling strength, and within the Born-Markov approximation, the master equation for the complete QD-cavity system (i.e., before adiabatic elimination) becomes

$$\frac{d\rho}{dt} = -\frac{i}{\hbar}[H_{\rm JC},\rho] + [L_\kappa(c) + L_\Gamma(|g\rangle\langle e|) + L_{2\gamma}(|e\rangle\langle e|) + L_\alpha(|e\rangle\langle p|)]\rho + \mathcal{K}_{\rm ph}(\rho), \quad \text{(B17)}$$

where the phonon-induced dissipator is given by

$$\mathcal{K}_{\rm ph}(\rho) = -\int_0^\infty ds\,{\rm Tr}_{\rm ph}[H_I,[\tilde{H}_I(-s),\rho(t)\rho_{\rm ph}]], \quad \text{(B18)}$$

where $\rm Tr_{ph}$ denotes a trace over the phonon modes. The interaction Hamiltonian is written

$$H_I = |e\rangle\langle e|\sum_k g_k(b_k^\dagger + b_k), \quad \text{(B19)}$$

where $b_k^\dagger$ is a creation operator for a phonon mode with wave vector k, and g_k describes its coupling strength to the QD exciton. The interaction-picture interaction Hamiltonian is defined by $\tilde{H}(-s) = e^{-iH_0 s}H_I e^{iH_0 s}$, where $H_0 = H_{\rm JC} + H_{\rm ph}$, with phonon Hamiltonian $H_{\rm ph} = \sum_k \omega_k b_k^\dagger b_k$ and ω_k the frequency of mode k. Finally, we assume a thermal state for the phonon density operator: $\rho_{\rm ph} = e^{-\beta H_{\rm ph}}/{\rm Tr_{ph}}(e^{-\beta H_{\rm ph}})$, with $\beta = \hbar/k_B T$ and T the sample temperature.

The strength of the QD-phonon coupling is characterized by the spectral density, defined as $J(\omega) = \sum_k g_k^2\delta(\omega-\omega_k)$, and which for excitons in QDs has been shown to be adequately described by the function

$$J(\omega) = \eta\,\omega^3\exp[-(\omega/\omega_c)^2], \quad \text{(B20)}$$

where η captures the overall strength of the interaction determined by material parameters, and ω_c is the photon cutoff frequency [42]. The behavior of the phonon dissipator in Eq. (B18) in different parameter regimes has been discussed in detail elsewhere [28–30]. The parameters used to obtain improved fits to the data in the main text (the solid orange curves in Fig. 4) are $\eta = 0.032$ meV^{-2} and $\omega_c = 1.3$ meV, while the constant pure-dephasing rate was reduced to $\gamma = 1$ μeV. These parameters correspond to phonons contributing approximately 40% of the dephasing on-resonance. We note that the other parameters in the model were adjusted to $1/\Gamma_B = 730$ ps and $g = 34$ μeV in order that the T_1 times as a function of detuning were well reproduced.

The density operator ρ entering Eq. (B17) contains both QD and cavity degrees of freedom. When relating the field operator $a(t)$ to the QD-cavity system, we have a choice to consider QD emission or cavity emission, making, respectively, the replacements $a \to c$ or $a \to |g\rangle\langle e|$ in the field correlation functions. Our data were better described by cavity emission, which we attribute to the high Purcell factor of our QD-cavity system.

[1] J.-W. Pan, Z.-B. Chen, C.-Y. Lu, H. Weinfurter, A. Zeilinger, and M. Żukowski, Rev. Mod. Phys. **84**, 777 (2012).
[2] P. Kok, W. J. Munro, K. Nemoto, T. C. Ralph, J. P. Dowling, and G. J. Milburn, Rev. Mod. Phys. **79**, 135 (2007).
[3] J. L. O'Brien, Science **318**, 1567 (2007).
[4] J. Nilsson, R. M. Stevenson, K. H. A. Chan, J. Skiba-Szymanska, M. Lucamarini, M. B. Ward, A. J. Bennett, C. L. Salter, I. Farrer, D. A. Ritchie *et al.*, Nat. Photon. **7**, 311 (2013).
[5] W. B. Gao, P. Fallahi, E. Togan, A. Delteil, Y. S. Chin, J. Miguel-Sanchez, and A. Imamoğlu, Nat. Commun. **4**, 2744 (2013).
[6] P. Michler, A. Kiraz, C. Becher, W. V. Schoenfeld, P. M. Petroff, L. Zhang, E. Hu, and A. Imamoglu, Science **290**, 2282 (2000).
[7] C. Santori, D. Fattal, J. Vuckovic, G. S. Solomon, and Y. Yamamoto, Nature (London) **419**, 594 (2002).
[8] E. B. Flagg, A. Muller, S. V. Polyakov, A. Ling, A. Migdall, and G. S. Solomon, Phys. Rev. Lett. **104**, 137401 (2010).
[9] P. Gold, A. Thoma, S. Maier, S. Reitzenstein, C. Schneider, S. Höfling, and M. Kamp, Phys. Rev. B **89**, 035313 (2014).
[10] M. Müller, S. Bounouar, K. D. Jöns, M. Glässl, and P. Michler, Nat. Photon. **8**, 224 (2014).
[11] Z. Yuan, B. E. Kardynal, R. M. Stevenson, A. J. Shields, C. J. Lobo, K. Cooper, N. S. Beattie, D. A. Ritchie, and M. Pepper, Science **295**, 102 (2002).
[12] T. Heindel, C. Schneider, M. Lermer, S. H. Kwon, T. Braun, S. Reitzenstein, S. Höfling, M. Kamp, and A. Forchel, Appl. Phys. Lett. **96**, 011107 (2010).
[13] D. J. P. Ellis, A. J. Bennett, S. J. Dewhurst, C. A. Nicoll, D. A. Ritchie, and A. J. Shields, New J. Phys. **10**, 043035 (2008).
[14] P. Yao, V. S. C. M. Rao, and S. Hughes, Laser Photon. Rev. **4**, 499 (2010).
[15] T. B. Hoang, J. Beetz, M. Lermer, L. Midolo, M. Kamp, S. Höfling, and A. Fiore, Opt. Express **20**, 21758 (2012).
[16] S. Reitzenstein and A. Forchel, J. Phys. D: Appl. Phys. **43**, 033001 (2010).
[17] O. Gazzano, S. Michaelis de Vasconcellos, C. Arnold, A. Nowak, E. Galopin, I. Sagnes, L. Lanco, A. Lematre, and P. Senellart, Nat. Commun. **4**, 1425 (2013).
[18] J. M. Gérard, B. Sermage, B. Gayral, B. Legrand, E. Costard, and V. Thierry-Mieg, Phys. Rev. Lett. **81**, 1110 (1998).
[19] J. Claudon, J. Bleuse, N. S. Malik, M. Bazin, P. Jaffrennou, N. Gregersen, C. Sauvan, P. Lalanne, and J.-M. Gerard, Nat. Photon. **4**, 174 (2010).
[20] M. E. Reimer, G. Bulgarini, N. Akopian, M. Hocevar, M. B. Bavinck, M. A. Verheijen, E. P. Bakkers, L. P. Kouwenhoven, and V. Zwiller, Nat. Commun. **3**, 737 (2012).
[21] M. Arcari, I. Söllner, A. Javadi, S. Lindskov Hansen, S. Mahmoodian, J. Liu, H. Thyrrestrup, E. H. Lee, J. D. Song, S. Stobbe *et al.*, Phys. Rev. Lett. **113**, 093603 (2014).
[22] Y.-M. He, Y. He, Y.-J. Wei, D. Wu, M. Atature, C. Schneider, S. Hofling, M. Kamp, C.-Y. Lu, and J.-W. Pan, Nat. Nano **8**, 213 (2013).

[23] A. Naesby, T. Suhr, P. T. Kristensen, and J. Mørk, Phys. Rev. A **78**, 045802 (2008).
[24] A. Auffeves, J.-M. Gérard, and J.-P. Poizat, Phys. Rev. A **79**, 053838 (2009).
[25] S. Varoutsis, S. Laurent, P. Kramper, A. Lemaître, I. Sagnes, I. Robert-Philip, and I. Abram, Phys. Rev. B **72**, 041303 (2005).
[26] A. Kiraz, M. Atatüre, and A. Imamoglu, Phys. Rev. A **69**, 032305 (2004).
[27] F. Troiani, J. I. Perea, and C. Tejedor, Phys. Rev. B **73**, 035316 (2006).
[28] P. Kaer, N. Gregersen, and J. Mork, New J. Phys. **15**, 035027 (2013).
[29] P. Kaer, P. Lodahl, A.-P. Jauho, and J. Mork, Phys. Rev. B **87**, 081308(R) (2013).
[30] P. Kaer and J. Mørk, Phys. Rev. B **90**, 035312 (2014).
[31] D. P. S. McCutcheon and A. Nazir, Phys. Rev. Lett. **110**, 217401 (2013).
[32] Y.-J. Wei, Y. He, Y.-M. He, C.-Y. Lu, J.-W. Pan, C. Schneider, M. Kamp, S. Höfling, D. P. S. McCutcheon, and A. Nazir, Phys. Rev. Lett. **113**, 097401 (2014).
[33] S. Weiler, A. Ulhaq, S. M. Ulrich, S. Reitzenstein, A. Löffler, A. Forchel, and P. Michler, Phys. Status Solidi (B) **248**, 867 (2011).
[34] M. Lermer, N. Gregersen, F. Dunzer, S. Reitzenstein, S. Höfling, J. Mørk, L. Worschech, M. Kamp, and A. Forchel, Phys. Rev. Lett. **108**, 057402 (2012).
[35] M. Munsch, A. Mosset, A. Auffèves, S. Seidelin, J. P. Poizat, J.-M. Gérard, A. Lemaître, I. Sagnes, and P. Senellart, Phys. Rev. B **80**, 115312 (2009).
[36] K. Hennessy, A. Badolato, M. Winger, D. Gerace, M. Atature, S. Gulde, S. Falt, E. L. Hu, and A. Imamoglu, Nature (London) **445**, 896 (2007).
[37] T. Grange, R. Ferreira, and G. Bastard, Phys. Rev. B **76**, 241304(R) (2007).
[38] We have also adjusted g and γ_B so that the T_1 data are well reproduced off-resonance.
[39] A. V. Kuhlmann, J. Houel, A. Ludwig, L. Greuter, D. Reuter, A. D. Wieck, M. Poggio, and R. J. Warburton, Nat. Phys. **9**, 570 (2013).
[40] H.-P. Breuer and F. Petruccione, *The Theory of Open Quantum Systems* (Oxford University Press, Oxford, 2002).
[41] H. J. Carmichael, *Statistical Methods in Quantum Optics* (Springer, New York, 1998).
[42] A. J. Ramsay, A. V. Gopal, E. M. Gauger, A. Nazir, B. W. Lovett, A. M. Fox, and M. S. Skolnick, Phys. Rev. Lett. **104**, 017402 (2010).